DEM simulations of critical state behaviour of granular materials under various drained triaxial stress path tests

Shiva Prashanth Kumar Kodicherla [1,*], Guobin Gong [2], Stephen Wilkinson[3]

[1] Department of Civil, Mining and Process Engineering, Namibia University of Science and Technology, Windhoek, Namibia

[2] Department of Civil Engineering, Xi'an Jiaotong-Liverpool University, China

[3] Faculty of Engineering and Information Sciences, University of Wollongong, Dubai

*Corresponding author. E-mail address: prashanthetc1024@gmail.com (S.P.K. Kodicherla);

Guobin.Gong@xjtlu.edu.cn (G. Gong); 2stephen.wilkinson@gmail.com (S.Wilkinson)

Abstract: The present study investigates the critical state behaviour of granular assemblies composed of clumped particles under four different drained axisymmetric triaxial stress paths, using the discrete element method (DEM). A series of numerical samples were prepared at initial states with different density indexes (I_D) and different initial confining pressures (p'_o). These samples were sheared to large strains, at which constant stresses and volumes were maintained to reach the critical state. The evolution of stress ratio under the same loading mode (for the same intermediate principal stress ratio, b) is shown to yield an almost identical behaviour independent of stress paths, whereas the stress-strain response depends on the stress paths. Four different axisymmetric stress paths all share the same unique friction angle at critical state, indicating the Mohr-Coulomb failure criterion is the appropriate critical state strength criterion, which is at least true for the axisymmetric stress conditions. A unique coordination number (CN) is achieved at the critical state for a given p'_o, which is independent of the stress path. The critical state CN is found to increase with the increase in p'_o, which could be attributed to the decrease in the critical state void ratio (e_c) as mean effective stress (p') increases. Interestingly, a unique linear functional relationship is found between the critical state values of CN and e_c, and a unique polynomial functional relationship is found between the critical state values of CN and p'. These functional relationships indicate no dependency on the stress paths or loading modes, thus characterizing unique features at critical states at both macroscopic and microscopic levels for a given type of granular material.

Keywords: Discrete element method; Critical state; Drained behaviour; Triaxial stress paths

Graphical abstract:

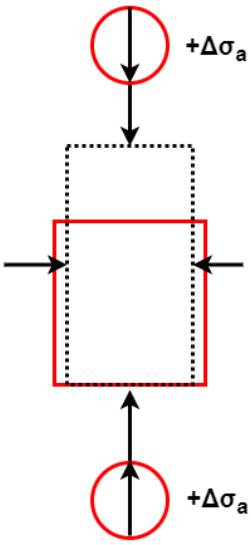

a) Axial Compression (AC)

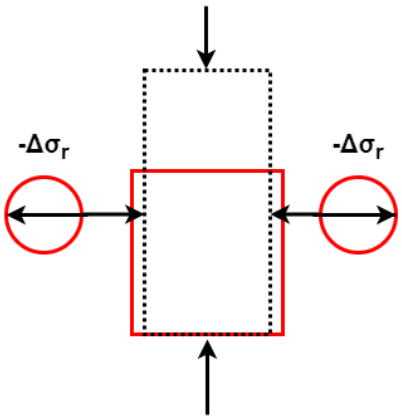

b) Lateral Extension (LE)

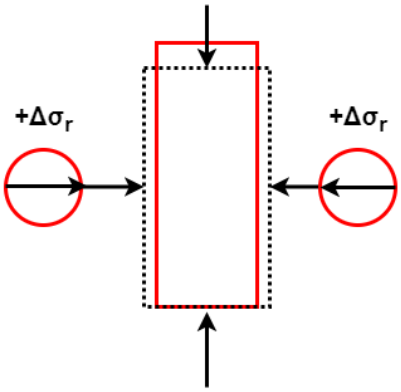

c) Lateral Compression (LC)

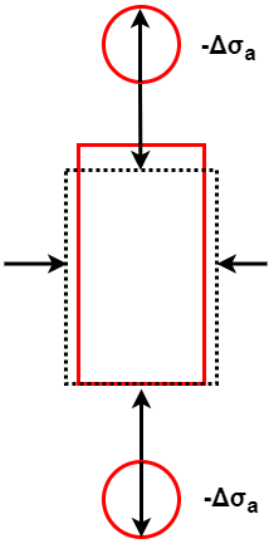

d) Axial Extension (AE)

Highlights:

- For axial compression (AC) stress path, a unique deviator stress, stress ratio and mean effective stress is achieved respectively at the critical state for a given initial confining pressure (p'_o).
- Independence of stress paths, a unique coordination number (CN) is achieved at the critical state for a given initial confining pressure.
- As the initial confining pressure increases, the critical CN will increase, and such an increase can be correlated to a decrease in the critical state void ratio (e_c).

- A unique linear relationship is found between the critical coordination numbers and the critical state void ratio.
- A unique polynomial relationship is found between the critical coordination numbers and mean effective stresses (p').

1. Introduction

The classical critical-state theory (CST) developed by Roscoe et al. (1958) and Schofield & Wroth (1968) laid the foundation for critical state soil mechanics (CSSM). The uniqueness of the critical state line (CSL) has been debated for many years and remains an open topic in the research community (e.g., Zhao & Guo, 2013; Yang & Wu, 2017). The critical state refers to the state of a soil sample deforming in shear with both the stress state and volume of the sample maintained as constant. The critical state line, comprised of critical states for a given soil under axisymmetric stress conditions, is characterized by a constant stress ratio $M = q/p'$, where p' and q commonly refer to the mean effective stress and deviator stress respectively, and M denotes the critical state stress ratio that may depend on the shear mode, for instance, with constant Lode angles of stress or constant intermediate principal stress ratios (Zhao & Guo, 2013). Xie et al. (2017) identified, from their simulation results, that critical state loci in the compression $e - p'$ space was slightly affected by the aspect ratio but the critical stress ratio was found to mainly depend on the aspect ratio and intermediate stress ratio. Yang & Wu (2017) showed that a unique critical state line (CSL) can be approximately obtained in $e - p'$ space, which seems to contradict earlier observations (Zhao & Guo, 2013; Yang & Wu, 2017). In addition, Li (2006) showed that the CSL in the $e - \log(p')$ space obtained in triaxial extension (TE) simulations was located above that obtained in triaxial compression (TC) indicating a non-unique CSL. However, most discrete element method (DEM) investigations have shown that the CSL is unique and independent of the initial states and loading conditions. Zhao & Evans (2011) showed that the locus of the CSL depended on the initial density and loading paths by comparing the simulation data from conventional triaxial, plane strain and direct shear tests using DEM. It can be inferred, from these discussions, that the uniqueness or non-uniqueness of the relationships between critical state strength parameters and stress path parameters is worth further investigations.

Springman et al. (2013) identified that several characteristic features, such as depression and extensions along with drainage conditions, may be more likely to lead to slope instabilities in the field. To mimic these characteristic features, more generalized loading conditions along with advanced testing devices such as the true triaxial apparatus were developed and these allowed the analysis of the intermediate principal stress on the shear strength of granular soils (e.g., Ko & Scott, 1968; Green & Bishop, 1969; Lade & Duncan, 1973; Reades & Green, 1976; Lam & Tatsuoka, 1988; Wang & Lade, 2001; Shapiro & Yamamuro, 2003). However, it is difficult to have the same initial soil samples which will be needed for subsequent experiments with different stress paths, and therefore the sample equivalence due to the different initial states including soil fabric could always be

questioned. In the recent past, the DEM has become a promising tool to investigate the mechanical behaviour of granular soils as an alternative, or complement, to physical experiments. Many researchers have applied DEM for analyzing the mechanical behaviour of granular materials under different loading conditions in relation to critical state behaviour (e.g., Ng, 2004, 2009; Huang et al., 2014; Fu & Dafalias, 2015; Yang & Wu, 2017; Xie et al., 2017; Ciantia et al., 2019; Li et al., 2020; Shi et al., 2021; Lin et al., 2022). However, the behaviour of granular materials is also affected by the different stress paths imposed (Jiang et al., 2013; Rodriguez & Lade, 2013). A more generalized three-dimensional stress state can be achieved using a true triaxial apparatus (TTA) (Ko & Scott, 1967; Green & Bishop, 1969; Head, 1986). Moreover, each stress path has its critical field significance and thus the following four stress paths are adopted in this investigation for simplicity (see Fig. 1):

- Axial compression (AC) – The specimen is loaded axially ($\Delta\sigma_a \uparrow$) while the initial confining pressure is kept constant ($\Delta\sigma_r = 0$).
- Axial extension (AE) – The specimen is unloaded axially ($\Delta\sigma_a \downarrow$) while the initial confining pressure is kept constant ($\Delta\sigma_r = 0$).
- Lateral compression (LC) – The specimen is loaded laterally ($\Delta\sigma_r \uparrow$) while the axial pressure is kept constant ($\Delta\sigma_a = 0$).
- Lateral extension (LE) – The specimen is unloaded laterally ($\Delta\sigma_r \downarrow$) while the axial pressure is kept constant ($\Delta\sigma_a = 0$).

Fig. 1

In addition to the above-discussed aspects related to the CSL, Kodicherla et al. (2019) demonstrated that particle shape is an important factor in the critical state behaviour of granular materials. In general, prior DEM simulations have employed both discs in two-dimensions and spheres in three-dimensions (e.g., Maeda et al., 2010), because of the lower computational cost and ease of contact detection (e.g., Ng, 2009; Sitharam & Vinod 2009; Yan & Dong, 2011). However, these may not represent the behaviour of true granular materials. Therefore, in the recent past, some DEM investigations considered various particle shapes, e.g., non-spherical particles such as spherocylinders (Pournin et al. 2005), ellipsoids (Ng 2009), clumped spheres (Hartl & Ooi 2011), superellipsoids (Wellmann et al. 2008; Cleary 2010) and polyhedrons (Zhao et al. 2015). However, at present, there is no standard shape that can represent a generalized framework for describing arbitrary particle geometry to simulate the true behaviour of granular materials.

The present paper addresses the disparities concerning the uniqueness of the CSLs previously discussed, based on a DEM simulation approach. The virtual samples used in this study are composed of a randomly chosen clumped particle generated using a multi-sphere approach in PFC3D. In total, 60 numerical samples were sheared comprising 3 different densities and 4 stress paths making a series of 12 simulations for each of the 5 initial confining pressures. The four different stress paths are axial compression (AC), axial extension (AE), lateral compression (LC) and lateral extension (LE). Each series represents 5 simulations with different initial

confining pressures p'_o , as 100 kPa, 200 kPa, 400 kPa, 800 kPa and 1600 kPa. All samples were sheared to the critical state and the influence of stress paths was investigated to examine the uniqueness of the CSLs. Moreover, the microscopic quantities in terms of coordination number (CN) and fabric anisotropy considering the deviator fabric, strong and weak force subnetworks are discussed.

2. Simulation details

Three-dimensional DEM simulations were performed by employing a commercial program named Particle Flow Code (PFC3D), developed by Itasca Consulting Group (2019) on a Dell Precision T7500 workstation, which has the following specifications: Intel® Xeon® CPU X5690 @3.47 GHz; 12 cores; 48 GB of RAM; NVIDIA Quadro 4000. To consider the representative behaviour of granular materials, a randomly selected clump template in the form of an STL file is modelled using the multi-sphere (MS) approach (Taghavi 2000). The following morphological descriptors were adopted: $\xi = 0.5$ representing the ratio of the smallest to the largest pebble diameter within a clump (i.e., particle geometry) and $\beta = 150°$ representing the maximum pebble-pebble intersection angle (i.e., particle surface texture), taking the computational limitations into account. More details on the effects of morphological descriptors of clumped particles are discussed by Kodicherla et al. (2019, 2020).

A cuboid assembly of dimensions 50 × 50 × 50 mm was modelled using rigid wall boundaries with each assembly limited to 2,845 clumped particles i.e., each clump consisting of 27 pebbles which means that a total of 76,815 pebbles in the whole assembly (see Fig. 2). The distribution of the equivalent diameter of the particle, where $d_{eq} = \sqrt{6V/\pi}$, in which V is the volume of a clump and the inset in Fig. 3 shows different orientations of the clumped particle.

Fig. 2, 3

In terms of clump-clump and clump-wall contact interactions, a simple linear force-displacement law was assigned, see also Yan (2009), Abedi & Mirghasemi (2011), Stahl & Konietzky (2011), Gu et al. (2014), Yang et al. (2016), Kodicherla et al. (2019) among others. The effective modulus and stiffness ratio were taken as E^* =1.0 × 10^8 Pa and k^* =4/3 (Goldenberg & Goldhirsch 2005), respectively. The mass density of a clump was considered as 2700 kg/m^3. To achieve various states of assemblies, different interparticle friction coefficients were assigned at the sample preparation phase and those were replaced by 0.5 during shearing. A density index ($I_D = \left(e_{up} - e\right) / \left(e_{up} - e_{low}\right)$) is used to classify the samples with different initial void ratios, to examine dilatancy and critical state behaviour. More details on how to achieve different density index (I_D) values are presented in Appendix A.

During the isotropic compression, a built-in stress-controlled servo mechanism was triggered to achieve the desired stress levels. The walls were permitted to move at a persistent loading rate of 0.004 m/s, which is small enough to ensure the existence of quasi-static shear (Zhao & Zhao 2019). Moreover, the assemblies were monitored by the inertia number (I), which is given by (da Cruz et al. 2005):

$$I = \dot{\varepsilon} d_i \sqrt{\rho_g / p'} \tag{1}$$

where $\dot{\varepsilon}$ is the axial strain rate, d_i is the diameter of the i^{th} particle, p' is mean effective normal stress and ρ_g is the particle density. Quasi-static shear can be achieved by a small value of I, thus I was maintained at a value less than 10^{-4} throughout the simulation. Further details on the choice of loading rate and loading scheme were discussed by Li et al. (2013).

3. Simulation program

In total, 60 numerical samples were sheared from 12 different series of numerical simulations to the critical state under various stress paths. In each stress path test, three different initial states of assemblies, i.e., loose, medium and dense based on their I_D values with five different p_o' (= 100, 200, 400, 800 and 1600 kPa) are considered. For loose, medium and dense soils, the I_D values vary from 15%–35%, 35%–65% and 65%–85%, respectively. All samples were found to reach a steady value under constant stress and volume beyond an axial strain level of approximately 40% which satisfies the classical definition of the critical state (Kodicherla et al., 2021). The summary of the initial characteristics of DEM assemblies is presented in Table 1.

Table 1

4. Results and discussion

All the samples obtained from the isotropic compression stage with varying initial confining pressures and densities are then sheared to the critical state under drained triaxial test conditions. Four modes of shear are considered in this investigation (i.e., AC, AE, LC and LE). All samples are sheared to large strains with constant stress and volume as the requirement of critical state theory (CST). The results are presented at both macroscopic and microscopic levels, and for Section 4.1, only the isotropically compressed samples at p_o'= 400 kPa are presented for brevity. The results for the other stress paths with varying p_o' exhibit similar behaviour.

4.1 Evolution of macroscopic behaviour

The macroscopic behaviour of granular materials during shearing can be evaluated using a Cauchy stress tensor (e.g., Christoffersen et al. 1981; Mehrabadi et al. 1982). Supplementary information on the stress tensor is furnished in Appendix B. The macroscopic behaviour of the AC stress path tests with different density indexes

is shown in Fig. 4. The loose sample (i.e., I_{Do}= 0.204) exhibits strain-hardening behaviour while the dense sample (i.e., I_{Do}= 0.741) shows initial hardening with a post-peak strain softening response (see Fig. 4(a)–(c)). The medium sample (i.e., I_{Do}= 0.514) exhibits initial hardening with minor post-peak strain-softening behaviour. For a given p'_o, a unique value of deviator stress, stress ratio and mean effective stress is achieved at the critical state. Also, similar observations were reported in DEM simulations of granular materials by Kodicherla et al. (2021).

The evolution of mobilized friction angle $\sin\phi = (\sigma_1 - \sigma_3)/(\sigma_1 + \sigma_3)$ for dense samples (i.e., I_{Do} = 0.741) under different stress paths is shown in Fig. 5. For an intuitive observation of the variations in $\sin\phi$, dense samples are considered. Although, the trend of $\sin\phi$ for AC followed the same trend as LE while AE followed the same trend as LC, an approximate unique value of $\sin\phi_{cs}$ = 0.48 at the critical state is identified. Moreover, the peak values of $\sin\phi$ under AE and LC were found to be higher than those of AC and LE.

The comparison of stress-strain behaviour of the granular assembly sheared under various stress paths is shown in Fig. 6. According to standard soil mechanics convention, the deviator stress $q = (\sigma_1 - \sigma_3)$ is positive for compression samples and negative for extension samples. If the absolute value of q is used to evaluate the stress ratio (as shown in Fig. 6(c)), the evolution of the stress ratio for AC is essentially the same as that for LE and similarly, the evolution of the stress ratio for AE is essentially the same as that for LC. Among the stress paths, LC is found to have the highest deviator stress against the axial strain (see Fig. 6(a)) and the volumetric strain for the AC sample followed that of the LC sample while the volumetric strain of the AE sample followed that of LE sample. The evolution of the stress ratio under the same loading mode with the same b yields an almost identical behaviour independent of stress paths, whereas the stress-strain response depends on the stress paths (see Fig. 6(b) and (c)).

Fig. 4, 5, 6

4.2 Evolution of critical state parameters

The relationship between critical state void ratio (e_c) and mean effective normal stress (p') can be expressed in $e - \log(p')$ space. The critical state framework usually assumes the existence of a unique critical state line (CSL) for a given soil sample in $e - q - p'$ space. The soil sample is expected to shear up to large strains under constant stress and volume. According to Roscoe & Burland (1968), and Schofield & Wroth (1968), the CSL was originally derived from the tests conducted on remoulded clays and it was found to be a straight line in $e - \log(p')$ space. However, this may not be true for real sands (Been et al. 1991; Verdugo & Ishihara 1996; Riemer & Seed 1997). Li & Wang (1998) proposed a linearization approach for describing the CSL in the $e - (p'/p_a)^{\xi}$ space, which can be expressed as:

$$e_c = \Gamma - \lambda\left(p' / p_a\right)^{\xi} \quad (2)$$

where Γ is the intercept of the CSL on the y-axis at $p' = 0$ and λ is the slope of CSL and ξ is the parameter used for fine-tuning during the optimization, taken as 0.7 and p_a is the atmospheric pressure serving as a reference pressure for normalization, which is taken as 101 kPa.

Fig. 7 shows the relationship between the void ratio (e_c) and the mean stress $\left(p' / p_a\right)$ at critical state for the stress paths (AC, AE, LC and LE), where the curve in the $e_c - \left(p' / p_a\right)$ space is found to depend on the stress paths and the relationship is not linear for any of the stress paths considered in the study. The huge scattering might be due to the clumped system/particle's morphological features and limited number of particles used.

Fig. 8 shows the relationship between the void ratio (e_c) and mean stress at a critical state for the stress paths (AC, AE, LC and LE), where the curve in the $e_c - (p' / p_a)^{0.7}$ space is found to depend on the stress paths and the relationship is linear for each stress path.

Based on the values of the intermediate principal stress ratio ($b = (\sigma_2 - \sigma_3)/(\sigma_1 - \sigma_3)$, where σ_1 is major principle stress, σ_2 is intermediate principle stress and σ_3 is minor principle stress), the critical state lines of AC & LE and LC & AE are grouped (i.e., the b values for AC & LE and LC & AE are 0 and 1 respectively). The critical state data points in $q - p'$ space are linearly fitted and considered to pass through the origin as presented in Fig. 9. The critical stress ratio (M) for AC & LE and LC & AE are found to be $M_{AC\&LE} = q/p' = 1.08$ and $M_{LC\&AE} = 0.78$, respectively. The ratio of $M_{AC\&LE}/M_{LC\&AE} = 1.38$ which is slightly high compared to the typical range of sand as discussed in the literature (Yoshimine et al. 1998; Yang et al. 2008; Kodicherla et al. 2021).

Fig. 7, 8, 9

4.3 Microscopic parameters

4.3.1 Coordination number (CN)

The coordination number, CN (=2C/N) is a key microscopic parameter to investigate the structural stability of granular assemblies, where C is the number of contacts in the assembly and N is the total number of particles. The number "2" indicates that each contact is formed by two entities. For a clumped system, the number of contacts refers to the contacts between clumps.

The evolution of CN against axial strain for all stress paths is shown in Fig. 10. For the extension stress path, there is an initial decline (i.e., ~10% axial strain) whereas for the compression path there is an initial increase and eventually both cases reach a critical value at large strain. Moreover, a unique value of CN is achieved at the critical state, which is found to be independent of the considered stress path for a given sample.

The relationships of CN against e_c and p' is presented in Fig. 11. Overall, a unique linear relationship between CN and e_c exists (see Fig. 11(a)), while a polynomial relationship is found between the CN and p' (see Fig. 11(b)). These functional relationships are unique and show no dependency on the stress paths or loading modes. In addition, the critical state CN is found to increase with the increase in mean p' at a critical state, corresponding to a decrease in e_c, the conclusion of which agrees with that reported by Kodicherla et al. (2020). Fig. 11 indicates that the fitting functions are empirical and statistical in nature, which are interestingly found to be unique. It is also interesting to find the intercept (when $p' = 0$) is 5.92 in the fitting equation of CN_{critical} against p', very close to 6, which is the limit value of CN for identifying granular instability for a frictionless system following the approach derived for a frictional granular system as provided by Zhu et al. (2021). However, such a macro-micro functional relationship is still an open question and it is not always feasible to associate the parameters or constants in such equations with a physical interpretation. More simulation or experimental data with general stress paths may be needed in order to better verify this point. In addition, the critical state is characterized by unique features at both macroscopic and microscopic levels and these plots show the unique correlations between the macroscopic and microscopic descriptors at the critical state.

Fig. 10, 11

4.3.2 Fabric anisotropy

The fabric of a granular assembly may evolve during the loading process. Thus, it is essential to understand the impact of fabric anisotropy on the mechanical behaviour of soils (Oda 1982; Yang et al. 2008; Fonseca et al. 2013). Supplementary information on the basic formulation of the fabric tensor and anisotropy in terms of deviator fabric is presented in Appendix C.

Fig. 12 presents the deviator fabrics against axial strain for overall, strong and weak deviator fabrics under four different stress paths. As can be seen from Fig. 12(a) at the critical state, a unique value of the overall deviator fabrics is achieved for AC & LE and LC & AE whereas for the strong and weak subnetworks, the deviator fabrics are biased. The magnitudes of deviator fabrics follow: $\phi_{d,overall} > \phi_{d,weak} > \phi_{d,strong}$, which means that the main contribution to the stress-fabric relationship is due to the strong force subnetworks only. Moreover, this observation agrees with the study in triaxial test simulations of granular materials by Thornton (2015).

All the critical deviator fabrics for overall, strong and weak subnetworks are presented in Fig. 13. The trends of overall deviator fabric are less scattered than those from the data points of strong and weak deviator fabrics for both compression and extension paths. Overall, the data points for all deviator fabrics seem to not correlate with p'/p_a. In this regard, the interpreted trends for AC & LE and LC & AE are illustrated for overall, strong and weak deviator fabric in Figs. 13(a, b and c), respectively. For the overall deviator fabric, an average of 0.171

with a coefficient of variance (CoV) of 0.048 for both (i.e., AC & LE and LC & AE) stress paths. Moreover, there is not much variation in the deviator fabrics of AC & LE and LC & AE.

Fig. 12, 13

5. Conclusions

The present study investigates the critical state behaviour of granular materials under different drained triaxial stress paths. Sixty numerical simulations were performed and their behaviours at macroscopic and microscopic levels are explored. Based on the observations, the following conclusions can be drawn:

(1) Unique values of deviator stress, stress ratio and mean effective stress are achieved at the critical state for a given initial confining pressure under an AC stress path.

(2) The evolution of stress ratio under the same loading mode (with the same value of the intermediate principal stress ratio, *b*) yields an almost identical behaviour regardless of stress paths, whereas the stress-strain responses (even with the same *b* value) are dependent on the loading mode.

(3) Independent of the stress paths, the mobilized friction angles are found to be approximately unique at the critical state.

(4) The critical stress ratio (*M*) is found to be dependent on the intermediate principal stress ratio *b*, and is higher under the AC & LE stress paths with *b* equal to 0 than under the AE & LC stress paths with *b* equal to 1.

(5) A unique coordination number (CN) is achieved at the critical state for a given initial mean effective stress $\left(p_o^{'}\right)$, which is independent of the stress paths, and the increase in critical CN corresponds to a decrease in the critical void ratio (e_c) as p_o' increases.

(6) A unique linear functional relationship is found between the critical state values of CN and e_c. Also, a unique polynomial functional relationship is found between the critical state values of CN and p'. These functional relationships show no dependency on the stress paths or loading modes, thus characterizing unique features for a given type of granular material.

It should be noted that, as mentioned in many previous investigations (e.g., Wood & Maeda 2008; Bandini & Coop 2011), there are significant gradation changes due to particle breakage or crushing that may occur in practical engineering, and therefore, the new soil may not be the same as the virgin one. Due to the limitation of the scope of the current investigation, especially concerning the levels of confining stresses, particle breakage is not considered. Moreover, although clumped particles can simulate particle shape effects to a certain degree, they cannot represent real sand without the mapping of the realistic particle shapes based on advanced image capture techniques such as 3D tomographic imagery. These may be worth future investigations.

Acknowledgements:

The financial support from Xi'an Jiaotong-Liverpool University (grant Nos. RDF 18-01-23, PGRS1906002 and REF-20-01-01) is gratefully acknowledged.

Appendix A. Densification index (I_D)

In soil mechanics, the state of soil can be well represented by relative density $D_r = (e_{max} - e) / (e_{max} - e_{min})$, where e_{max} and e_{min} are the maximum and minimum void ratios, respectively. However, in DEM simulations, the evaluation of e_{max} and e_{min} is challenging due to the continuous change in void ratio with different interparticle friction coefficient values during the sample preparation phase. Therefore, an alternative measure of D_r, is the densification index (I_D), which is used to capture the state of the numerical assembly. The expression for I_D is defined as (Zhang et al. 2018):

$$I_D = \frac{e_{up} - e}{e_{up} - e_{low}} \tag{A1}$$

where e_{up} and e_{low} are the corresponding void ratios of the upper and lower consolidation lines, respectively. The upper boundary is the isotropic consolidation line (*ICL*) of the loosest sample and the lower boundary is the *ICL* of a sample exposed to the densest state or maximum densification. It should be mentioned that the state of the sample in the DEM is mainly contingent on the application of the interparticle friction coefficient during specimen generation, or during the isotropic compression phase. To achieve the densest state, the zero interparticle friction coefficient should be assigned to the particles during the specimen generation phase, and then the *e* obtained at the end of the isotropic compression phase will be considered as e_{min}. Similarly, for the loosest state, the interparticle friction coefficient in the successive isotropic compression phase shall be gradually increased until the *e* becomes almost constant. The *e* obtained during this isotropic compression phase will be regarded as e_{max}.

Appendix B. Stress tensor

For a given representative elementary volume (REV), the macroscopic behaviour of granular material can be quantitatively obtained using averaged Cauchy's stress tensor (e.g., Christoffersen et al. 1981; Mehrabadi et al. 1982):

$$\sigma_{ij} = \frac{1}{V} \sum_{c \in V} f_i^c b_j^c \tag{B1}$$

where V is the total volume of the REV, f^c and b^c are the contact force and branch vectors at each contact point c, respectively. In addition, a contact force f^c can be decomposed into three sub-components, i.e., f_n^c, f_t^c and f_s^c in the n, t and s directions (in 3D) such that $f^c = f_n^c n + f_t^c t + f_s^c s$. Here, n, t and s are three orthogonal unit vectors parallel and perpendicular to the contact plane. The mean and deviator stresses are $p = \sigma_{ii}/3$ and $q = \sqrt{(3/2)s_{ij}s_{ij}}$ with $s_{ij} = \sigma_{ij} - p\delta_{ij}$, respectively, where δ_{ij} is the Kronecker delta. However, in this investigation, the average stresses are obtained directly from the wall forces which is a straightforward technique usually employed in PFC (Kodicherla et al. 2019, 2020).

Appendix C. Fabric tensors

Fabric refers to the spatial arrangement of particles and associated pore voids (Oda 1982). While shearing, the spatial arrangements of particles and void spaces tend to exhibit an extent of anisotropy and evolve to a specifically preferred orientation (Yimsiri & Soga 2011). Among the various definitions available for the fabric tensor (e.g., Oda 1982; Satake 1982; Li & Li 2009), a commonly used approach is the contact-normal based proposition, which can be expressed as:

$$\phi_{ij} = \frac{1}{N_c}\sum_{k=1}^{N_c} n_i^k n_j^k = \begin{bmatrix} \phi_{11} & \phi_{12} & \phi_{13} \\ \phi_{21} & \phi_{22} & \phi_{23} \\ \phi_{31} & \phi_{32} & \phi_{33} \end{bmatrix} \tag{C1}$$

where n^k = the contact unit normal vector of the contact k with $i, j = 1,2,3$ and N_c is the number of contacts in the assembly. The components ϕ_{11}, ϕ_{22} and ϕ_{33} are the fabric in the principal directions $(i = j)$, and ϕ_{12}, ϕ_{13}, ϕ_{21}, ϕ_{23}, ϕ_{31} and ϕ_{32} are the fabric components in the shear direction $(i \neq j)$. The scalar values of shear components in the opposite direction are equal, that is, $\phi_{12} = \phi_{21}$, $\phi_{13} = \phi_{31}$ and $\phi_{23} = \phi_{32}$. The principal values ϕ_1, ϕ_2, & ϕ_3 and principal directions of the fabric can be obtained by the eigenvalues and eigenvectors of the fabric tensor. According to Thornton (2000), the deviator fabric, $\phi_d\,(=\phi_1 - \phi_3)$, is the difference between major and minor principal fabric components i.e., the maximum and minimum eigenvalues of ϕ_{ij}, which is widely used to quantify the structural anisotropy of granular assemblies.

The whole contact network is distinguished into strong and weak subnetworks based on whether the normal contact force is higher or lower than the average normal contact force f_{avg}^n, respectively (Thornton & Anthony 1998). A similar decomposition approach was used in this investigation to distinguish the strong and weak force fabric networks. The average normal contact force is defined as:

$$f_{avg}^{n} = \frac{1}{N_c}\sum_{1}^{N_c} f_i^{n} \tag{C2}$$

where f_i^{n} is the i^{th} normal contact force. Based on the definition of fabric tensor mentioned in Eq. (C1), the associated fabric tensors with the subnetworks can be expressed as:

$$\phi_{ij}^{s} = \frac{1}{N_c^{s}}\sum_{k=1}^{N_c^{s}} n_i^{k}\, n_j^{k}, \qquad \phi_{ij}^{w} = \frac{1}{N_c^{w}}\sum_{k=1}^{N_c^{w}} n_i^{k}\, n_j^{k} \tag{C3}$$

where N_c^{s} and N_c^{w} are numbers of contacts in the strong and weak subnetworks, respectively. The total number of contacts N_c in the granular assembly is $N_c = N_c^{s} + N_c^{w}$.

References

Abedi, S. & Mirghasemi, A.A. (2011). Particle shape consideration in numerical simulation of assemblies of irregularly shaped particles. *Particuology*, *9*(4), 387-397.

Bandini, V. & Coop, M.R. (2011). The influence of particle breakage on the location of the critical state line of sands. *Soils and Foundations*, 51(4), 591-600.

Been, K., Jefferies, M.G. & Hachey, J. (1991). The critical state of sands. *Geotechnique*, 41(3), 365–381.

Ciantia, M.O., Arroyo, M., O'Sullivan, C., Gens, A. & Liu, T. (2019). Grading evolution and critical state in a discrete numerical model of Fontainebleau sand. *Geotechnique*, 69(1), 1-15.

Christoffersen, J., Mehrabadi, M.M. & Nemat-Nasser, S. (1981). A micromechanical description of granular material behaviour. *Journal of Applied Mechanics*, 48, 339-344.

Cleary, P.W. (2010). DEM prediction of industrial and geophysical particle flows. *Particuology*, 8, 106–118.

da Cruz, F., Emam, S., Prochnow, M., Roux, J.N. & Chevoir, F. (2005). Rheophysics of dense granular materials: discrete simulation of plane shear flows. *Physical Review: E*, 72(2), 021309.

Fonseca, J., O'Sullivan, C., Coop, M.R. & Lee, P. (2013). Quantifying the evolution of soil fabric during shearing using directional parameters. *Geotechnique*, 63(10), 487–499.

Fu, P. & Dafalias, Y.F. (2015). Relationship between void-and contact normal based fabric tensors for 2D idealized granular materials. *International Journal of Solids and Structures*, 63, 68–81.

Goldenberg, C. & Goldhirsch, I. (2005). Friction enhances elasticity in granular solids. *Nature*, 435(7039), 188–191.

Green, G. E. & Bishop, A. W. (1969). A note on the drained strength of sand under generalized strain conditions. *Geotechnique*, 19(1), 144–149.

Gu, X.Q., Huang, M.S. & Qian, J.G. (2014). DEM investigation on the evolution of microstructure in granular soils under shearing. *Granular Matter*, 16(1), 91-106.

Hartl, J. & Ooi, J.Y. (2011). Numerical investigation of particle shape and particle friction on limiting bulk friction in direct shear tests and comparison with experiments. *Powder Technology*, 212(1), 231-239.

Head, K.H. (1986). Manual of soil laboratory testing. Pentech Press, London.

Huang, X., Hanley, K. J., O'Sullivan, C., Kwok, C. Y. & Wadee, M. A. (2014). DEM analysis of the influence of the intermediate stress ratio on the critical-state behaviour of granular materials. *Granular matter*, 16, 641–655.

Itasca. (2019). PFC3D: Theory and background. Itasca Consulting Group.

Jiang, M.J., Li, L. & Yang, Q. (2013). Experimental investigation on deformation behavior of TJ-1 lunar soil simulant subjected to principal stress rotation. *Advanced Space Research*, 52, 136–146.

Ko, H.Y. & Scott, R. F. (1968). Deformation of sand at failure. *Journal of Soil Mechanics and Foundations Division*, 94(4), 883–898.

Ko, H.Y. & Scott, R.F. (1967). A new soil testing apparatus. *Géotechnique*, 17, 40–57.

Kodicherla, S. P. K., Gong, G., Fan, L. & Moy, C. K. S. (2019). Effects of particle morphology on the macroscopic behaviour of ellipsoids: A discrete element investigation. *Proceedings of the 2nd International Conference on Sustainable Buildings and Structures (ICSBS 2019)*, Papadikis et al. (Eds), Suzhou, China. pp. 45–50.

Kodicherla, S.P.K., Gong, G., Fan, L., Wilkinson, S. & Charles K.S. Moy. (2021). Discrete element modelling of strength and critical state characteristics of granular materials under axial compression and axial extension stress path tests. *Particuology*, 56,152-162.

Kodicherla, S.P.K., Gong, G., Fan, L., Wilkinson, S. & Moy, C.K.S. (2020). DEM investigations of the effects of particle morphology on granular material behaviour using a multi-sphere approach. *Journal of Rock mechanics and Geotechnical Engineering*, 12(6), 1301-1312.

Kodicherla, S.P.K., Gong, G., Yang, Z.X., Krabbenhoft, K., Fan, L. Moy, C.K.S. & Wilkinson, S. (2019). The influence of particle elongations on direct shear behaviour of granular materials using DEM. *Granular Matter*, 21, 86.

Lade, P. V. & Duncan, J.M. (1973). Cubical triaxial tests on cohesionless soil. *Journal of Soil Mechanics and Foundations Division*, 99 (10), 793–812.

Lam, W.K. & Tatsuoka, J. A. (1988). Effects of initial anisotropic fabric and sigma 2 on strength and deformation characteristics of sand. *Soils and Foundations*, 28(1), 89–106.

Li, X. & Li, X.S. (2009). Micro-macro quantification of the internal structure of granular materials. *Journal of Engineering Mechanics*, 135(7), 641–656.

Li, X. (2006). Micro-scale investigation on the quasi-static behavior of granular material. Doctorial Dissertation, Hong Kong University of Science and Technology.

Li, X. S. & Wang, Y. (1998). Linear representation of steady-state line for sand. *Journal of Geotechnical and Geoenvironmental Engineering*, 124(12), 1215–1217.

Li, X., Yu, H. S. & Li, X. S. (2013). A virtual experiment technique on the elementary behaviour of granular materials with discrete element method. *International Journal of Numerical and Analytical Methods in Geomechanics*, 37(1), 75–96.

Lin, M., Zhou, W., Liu, J., Ma, G. & Cao, X. (2022). A topological view on microscopic structural evolution for granular material under loading and unloading path. *Computers and Geotechnics*, 141, 10530.

Li, Y., Wu, W., Chu, X. & Zou, W. (2020). Effects of stress paths on triaxial compression mechanical properties of QH‐E lunar soil simulant studied by DEM simulation. *Granular matter*, 22, 32.

Maeda, K., Sakai, H., Kondo, A., Yamaguchi, T., Fukuma, M. & Nukudani, E. (2010). Stress–chain based micromechanics of sand with grain shape effect. *Granular Matter*, 12, 499–505.

Mehrabadi, M.M., Nemat-Nasser, S. & Oda, M. (1982). On statistical description of stress and fabric in granular materials. *International Journal of Numerical and Analytical Methods in Geomechanics*, 6, 95-108.

Ng, T. T. (2009). Discrete element method simulations of the critical state of a granular material. *International Journal of Geomechanics*, 9(5), 209–216.

Ng, T.T. (2004). Shear strength of assemblies of ellipsoidal particles. *Geotechnique*, 50(10), 659-669.

Oda, M. (1982). Fabric tensor for discontinuous geological materials. *Soils and Foundations*, 22(4), 96–108.

Pournin, L., Weber, M., Tsukahara, M., Ferrez, J. A., Ramaioli, M. & Liebling, T.M. (2005). Three-dimensional distinct element simulation of spherocylinder crystallization. *Granular Matter*, 7, 119–126.

Reades, D.W. & Green, G. E. (1976). Independent stress control triaxial extension tests on sand. *Geotechnique*, 26(4), 551–576.

Riemer, M. F. & Seed, R.B. (1997). Factors affecting apparent position of steady-state line. *Journal of Geotechnical and Geoenvironmental Engineering*, 123(3), 281.

Rodriguez, N.M. & Lade, P.V. (2013). Effects of principal stress directions and mean normal stress on failure criterion for cross-anisotropic sand. *Journal of Engineering Mechanics*, 139(11), 1592–1601.

Roscoe, K. & Burland, J.B. (1968). On the generalized stress-strain behavior of wet clay. Engineering Plasticity, J. Heyman and F. A. Leckie, eds., Cambridge University Press, Cambridge, U.K., 535–609.

Roscoe, K.H., Schofield, A.N. & Wroth, C.P. (1958). On the yielding of soils. *Geotechnique*, 8(1), 22-53.

Satake, M. (1982). Fabric tensor in granular materials. In Proceedings of the IUTAM Symposium on Deformations and Failure of Granular Materials 1982 (Vermeer PA and Luger HJ (eds)). Balkema, Rotterdam, the Netherlands, pp. 63–68.

Schofield, A. & Wroth, P. (1968). Critical state soil mechanics, McGraw-Hill, London.

Shapiro, S. & Yamamuro, J.A. (2003). Effects of silt on three-dimensional stress–strain behavior of loose sand. *Journal of Geotechnical and Geoenvironmental Engineering*, 129(1), 1–11.

Shi, D.D., Cao, D., Deng, Y.B. & Xue, J.F. (2021). DEM investigations of the effects of intermediate principal stress ratio and particle breakage on the critical state behaviors of granular soils. *Powder Technology*, 379, 547- 559.

Sitharam, T.G. & Vinod, J.S. (2009). Critical state behaviour of granular materials from isotropic and rebounded paths: DEM simulations. *Granular Matter*, 11 (1), 33–42.

Springman, S.M., Yamamoto, Y., Buchli, T., Hertrich, M., Maurer, H., Merz, K., Gartner-Roer, I. & Seward, L. (2013). Rock glacier degradation and instabilities in the European Alps: a characterisation and monitoring experiment in the Turtmanntal, CH. In Landslide Science and Practice. Edited by C. Margottini, P. Canuti, and K. Sassa. Springer, Berlin, Heidelberg, pp. 5–13.

Stahl, M. & Konietzky, H. (2011). Discrete element simulation of ballast and gravel under special consideration of grain-shape, grain-size and relative density. *Granular Matter*, 13(4), 417-428.

Taghavi, R. (2000). Automatic Block Decomposition Using Fuzzy Logic Analysis. *Proceedings of the 9th International Meshing Roundtable*, pp. 187–192. New Orleans: Sandia National Laboratories.

Thornton, C. & Antony, S. J. (1998). Quasi-static deformation of particulate media. *Proceedings of Royal Society A.* 356, 2763-2782.

Thornton, C. (2000). Numerical simulations of deviatoric shear deformation of granular media. *Geotechnique*, 50(1), 43-53.

Thornton, C. (2015). Granular Dynamics, Contact Mechanics and Particle System Simulations (Particle Technology Series). Hardcover – 15 September 2015.

Verdugo, R. & Ishihara, K. (1996). The steady state of sandy soils. *Soils and Foundation*, 36(2), 81–91.

Wang, Q. & Lade, P. V. (2001). Shear banding in true triaxial tests and its effect on failure in sand. *Journal of Engineering Mechanics*, 127(8), 754–761.

Wellmann, C., Lillie, C. & Wriggers, P. (2008). Comparison of the macroscopic behavior of granular materials modeled by different constitutive equations on the microscale. *Finite Elements in Analysis and Design*, 44, 259–271.

Wood, D.M. & Maeda, K. (2008). Changing grading of soil: Effect on critical states. *Acta Geotechnica*, 3(1), 3-14.

Xie, Y. H., Yang, Z. X., Barreto, D. & Jiang, M.D. (2017). The influence of particle geometry and the intermediate stress ratio on the shear behavior of granular materials. *Granular matter*, 19, 35.

Yan, W.M. & Dong, J. (2011). Effect of particle grading on the response of an idealized granular assemblage. *International Journal of Geomechanics*, 11, 276–285.

Yan, W.M. (2009). Fabric evolution in a numerical direct shear test. *Computers and Geotechnics*, 36(4), 597-603.

Yang, Z. X. & Wu, Y. (2017). Critical State for Anisotropic Granular Materials: A Discrete Element Perspective. *International Journal of Geomechanics*, 17(2), 04016054.

Yang, Z.X., Li, X.S. & Yang, J. (2008). Quantifying and modelling fabric anisotropy of granular soils. *Geotechnique*, 58(4), 237–248.

Yimsiri, S. & Soga, K. (2011). Effects of soil fabric on behaviors of granular soils: Microscopic modeling. *Computers and Geotechnics*, 38, 861–874.

Yoshimine, M., Ishihara, K. & Vargas, W. (1998). Effects of principal stress direction and intermediate principal stress on undrained shear behavior of sand. *Soils and Foundations*, 38(3), 179-188.

Zhang, J., Lo, S.C.R., Rahman, M.M. & Yan, J. (2018). Characterizing monotonic behavior of pond ash within critical state approach. *Journal of Geotechnical and Geoenvironmental Engineering*, 144(1), 04017100.

Zhao, J. & Guo, N. (2013). Unique critical state characteristics in granular media considering fabric anisotropy. *Geotechnique*, 63(8), 695–704.

Zhao, S. & Zhao, J. (2019). A poly-superellipsoid-based approach on particle morphology for DEM modeling of granular media. *International Journal for Numerical and Analytical Methods in Geomechanics*, 43(13), 2147-2169.

Zhao, S., Zhou, X. & Liu W. (2015). Discrete element simulations of direct shear tests with particle angularity effect. *Granular matter*, 17, 793-806.

Zhao, X. & Evans, T.M. (2011). Numerical analysis of critical state behaviors of granular soils under different loading conditions. *Granular Matter*, 13, 751–764.

Zhu, M., Gong, G., Xia, J., Liu, L. & Wilkinson, S. (2021). Effects of deviator strain histories on liquefaction of loose sand using DEM. *Computers and Geotechnics*, 136, 104213.

Figures:

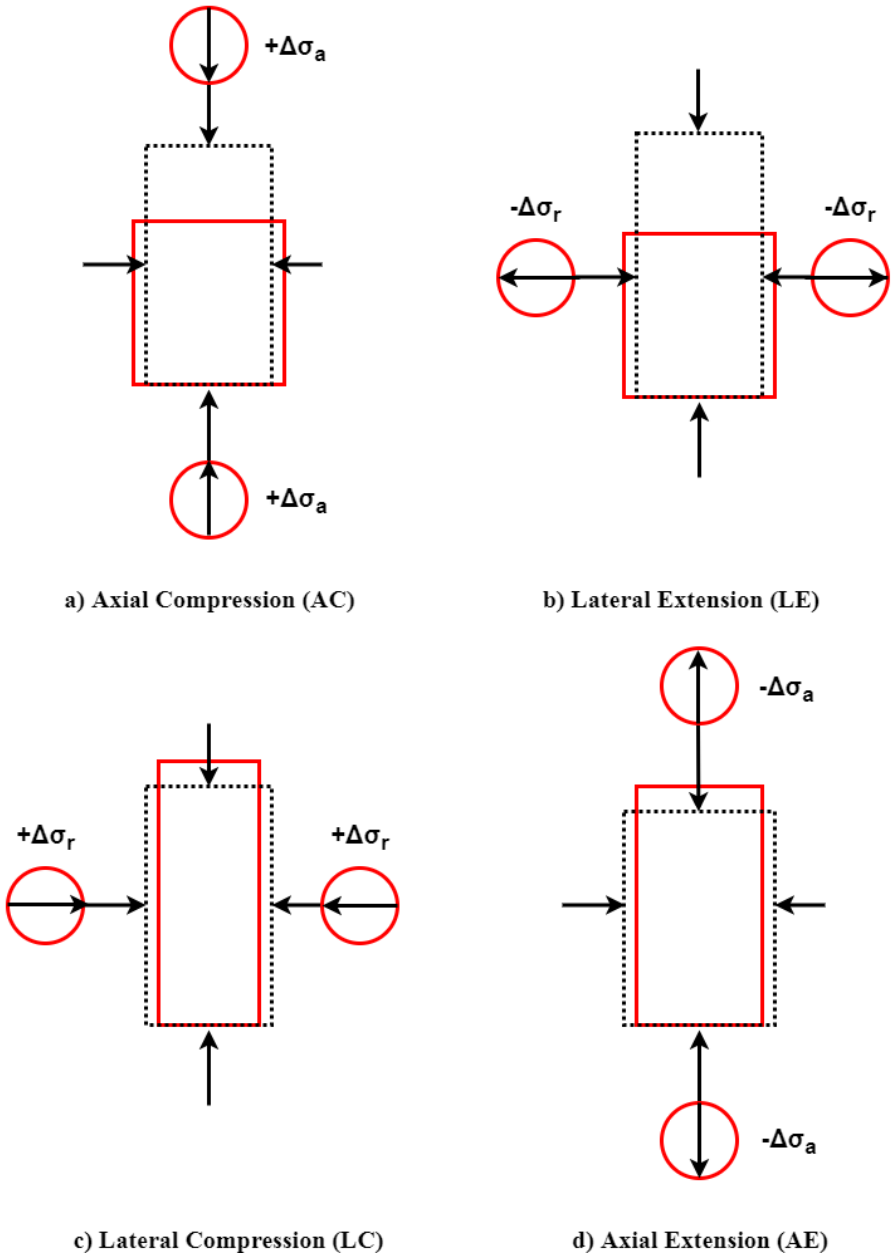

Fig. 1. Schematic representation of drained triaxial stress path tests (after Springman et al. 2013).

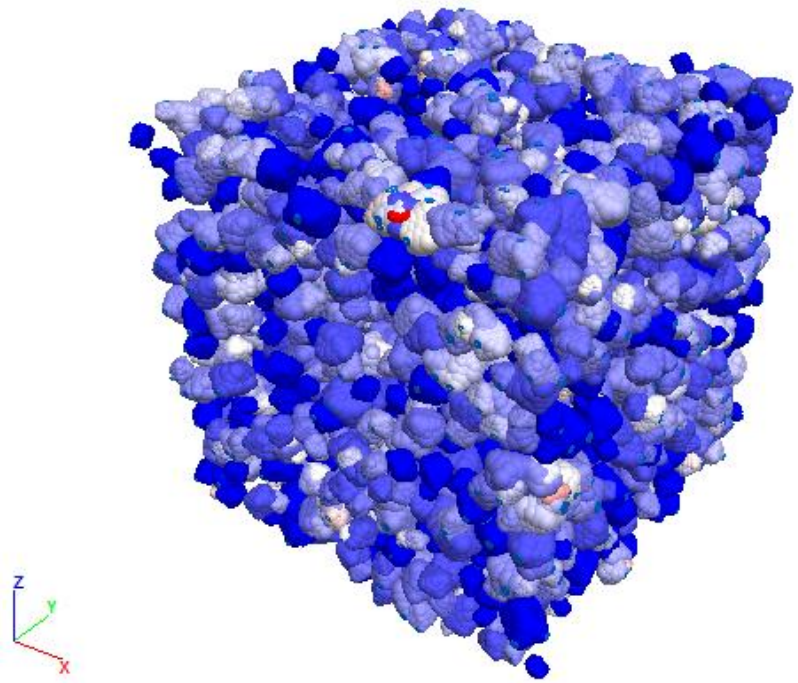

Fig. 2. Initial loose cubic packing of the DEM specimen (walls omitted).

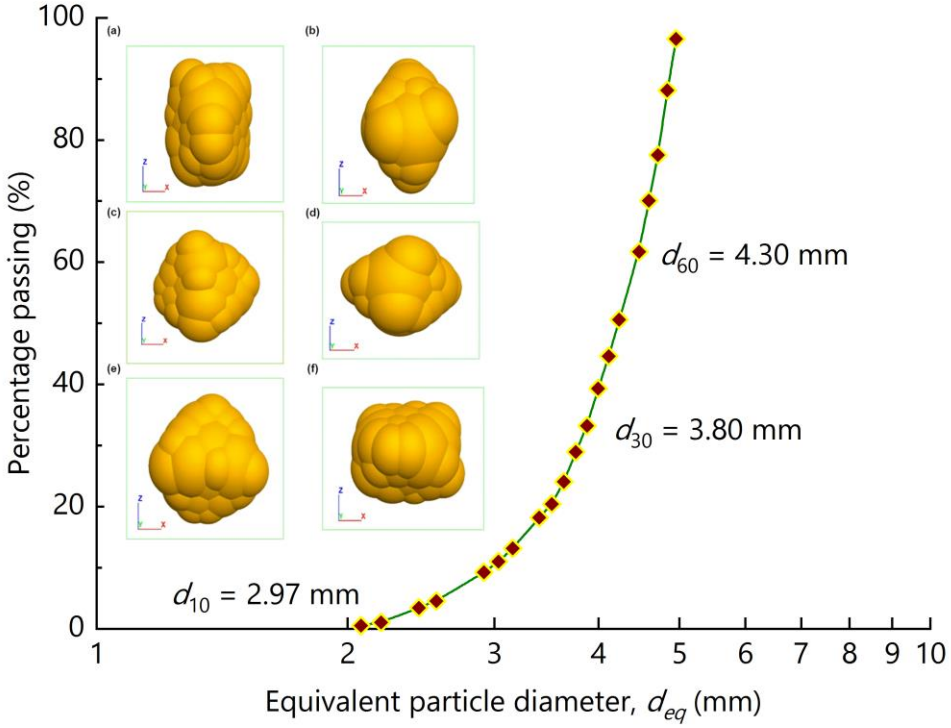

Fig. 3. Grain size distribution of the DEM assembly.

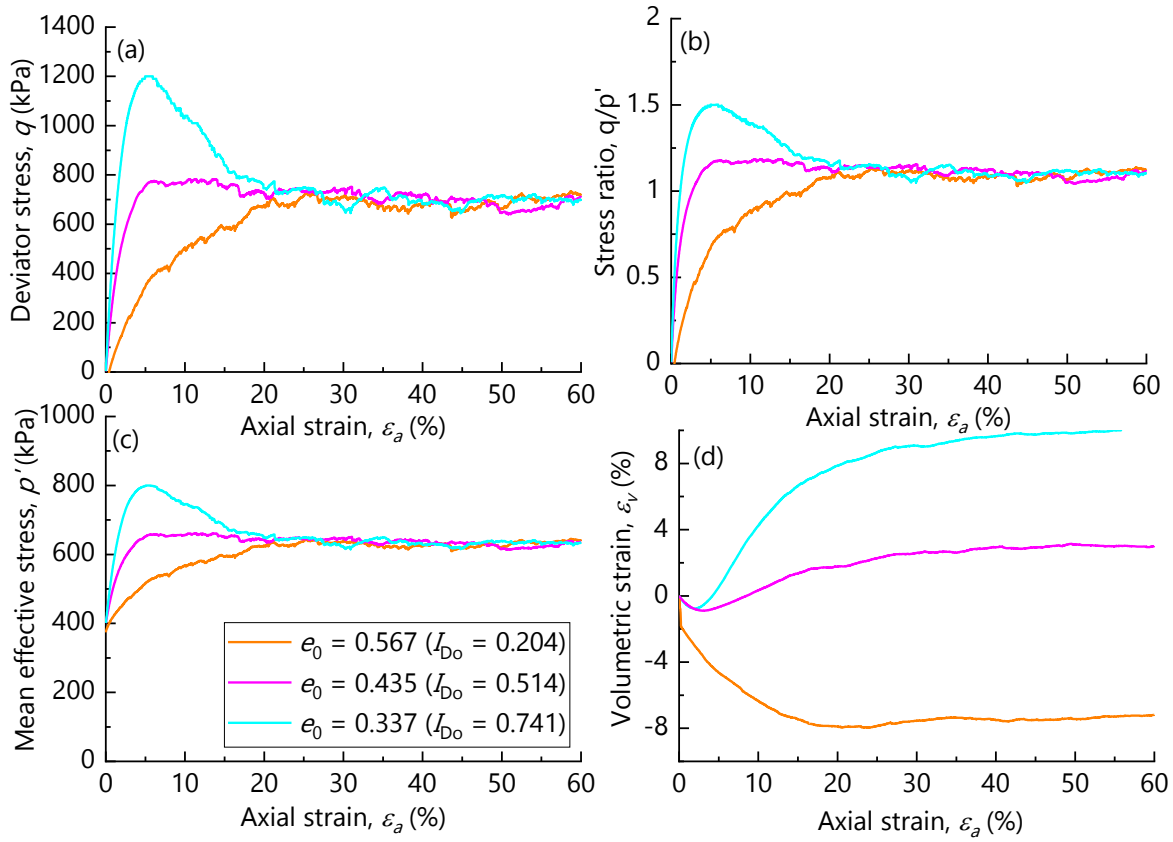

Fig. 4. Macroscopic behaviour of AC stress path test with different initial density values: (a) $q \sim \varepsilon_a$; (b) $q / p' \sim \varepsilon_a$; (c) $p' \sim \varepsilon_a$; (d) $\varepsilon_v \sim \varepsilon_a$.

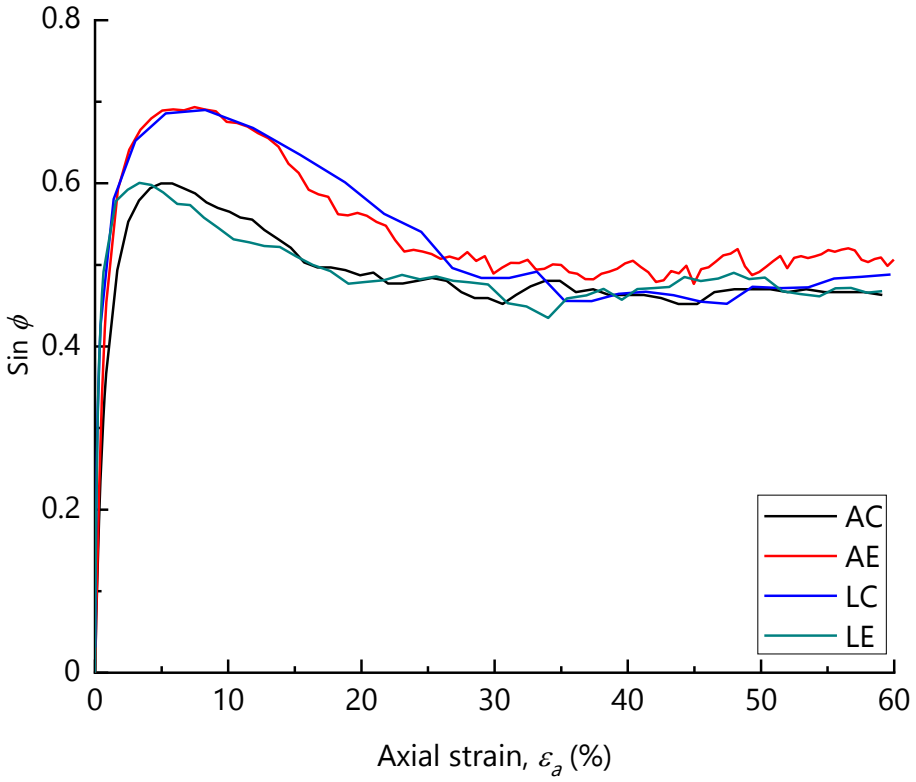

Fig. 5. Evolution of $sin\,\phi$.

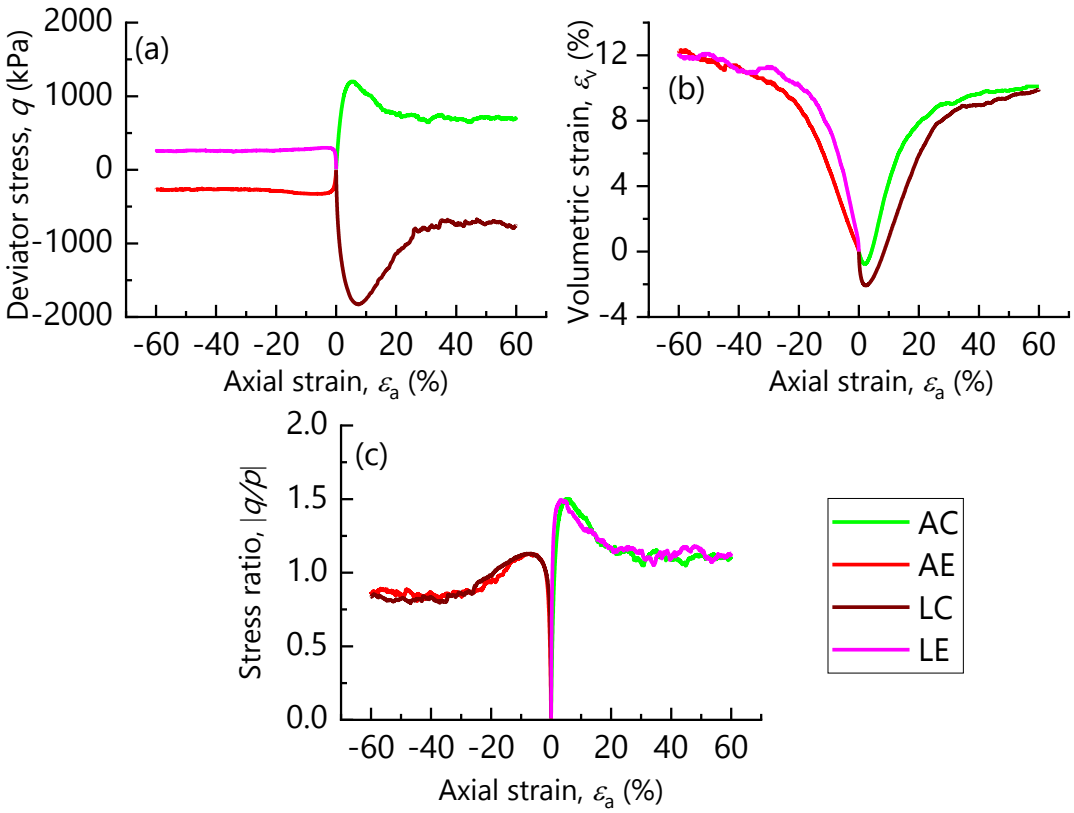

Fig. 6. Comparison of macroscopic behaviours: (a) $q \sim \varepsilon_a$; (b) $\varepsilon_v \sim \varepsilon_a$; (c) $q / p' \sim \varepsilon_a$.

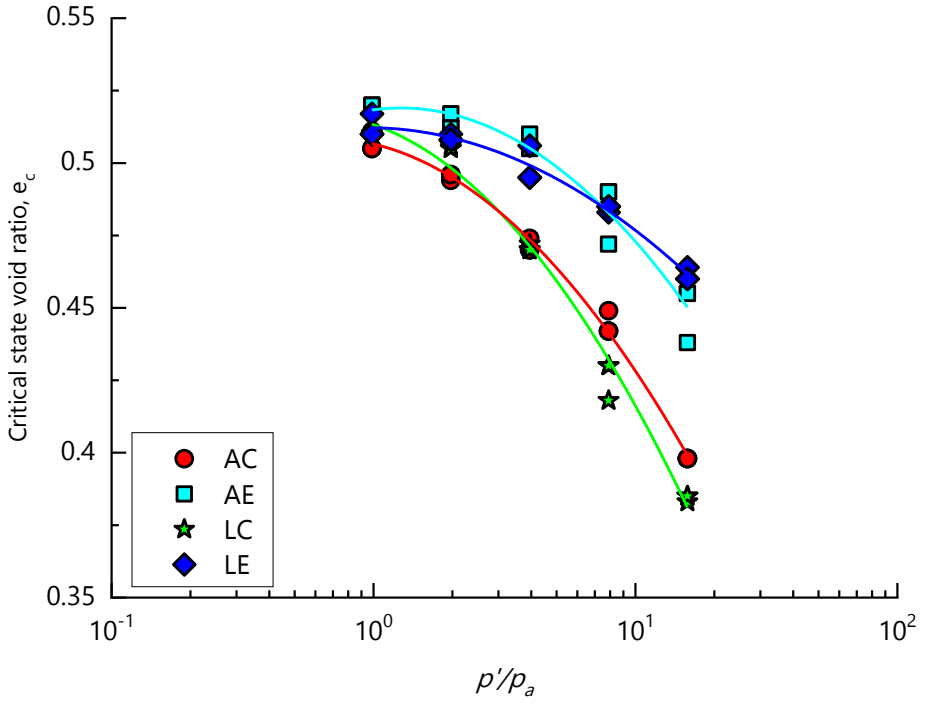

Fig. 7. Relationship between void ratio and mean effective stress at the critical state.

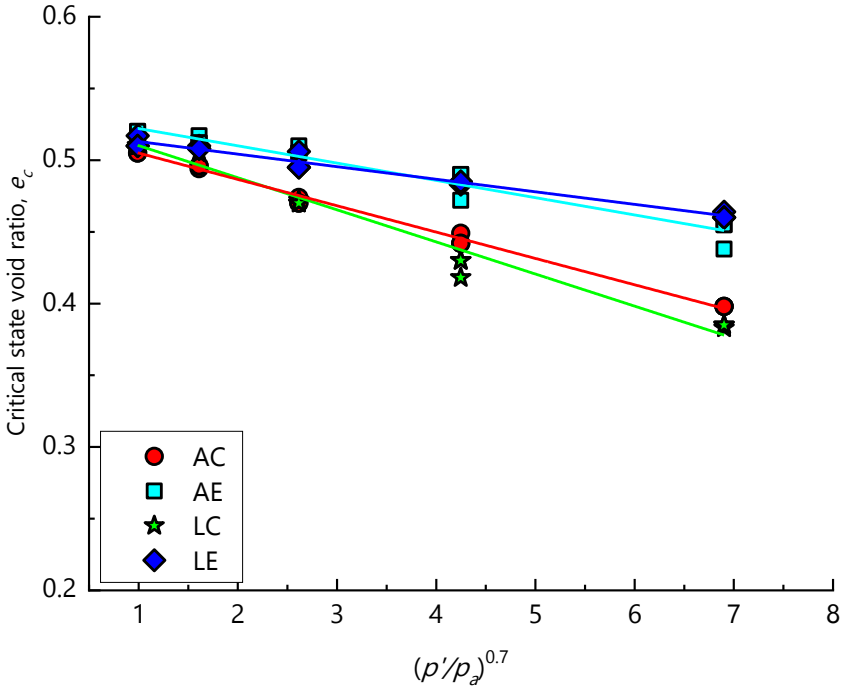

Fig. 8. Relationship between void ratio and mean stress at the critical state.

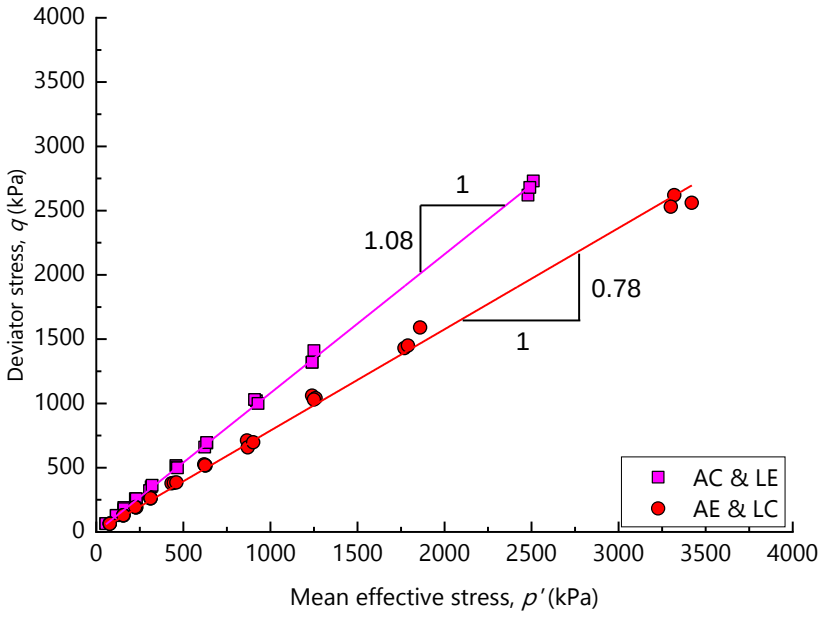

Fig. 9. Critical state lines in the $q - p'$ space.

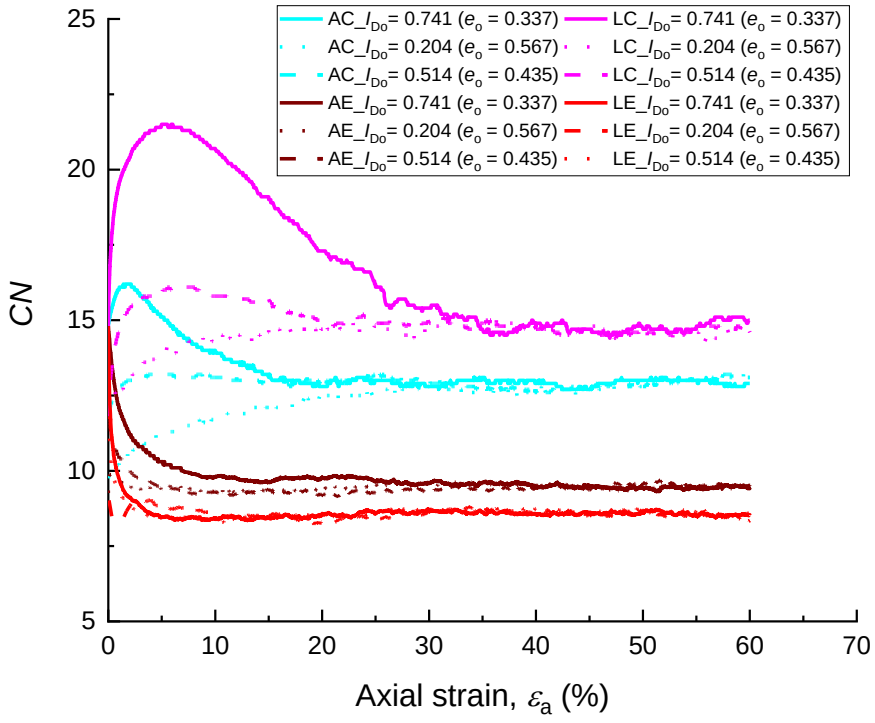

Fig. 10. Evolution of CN.

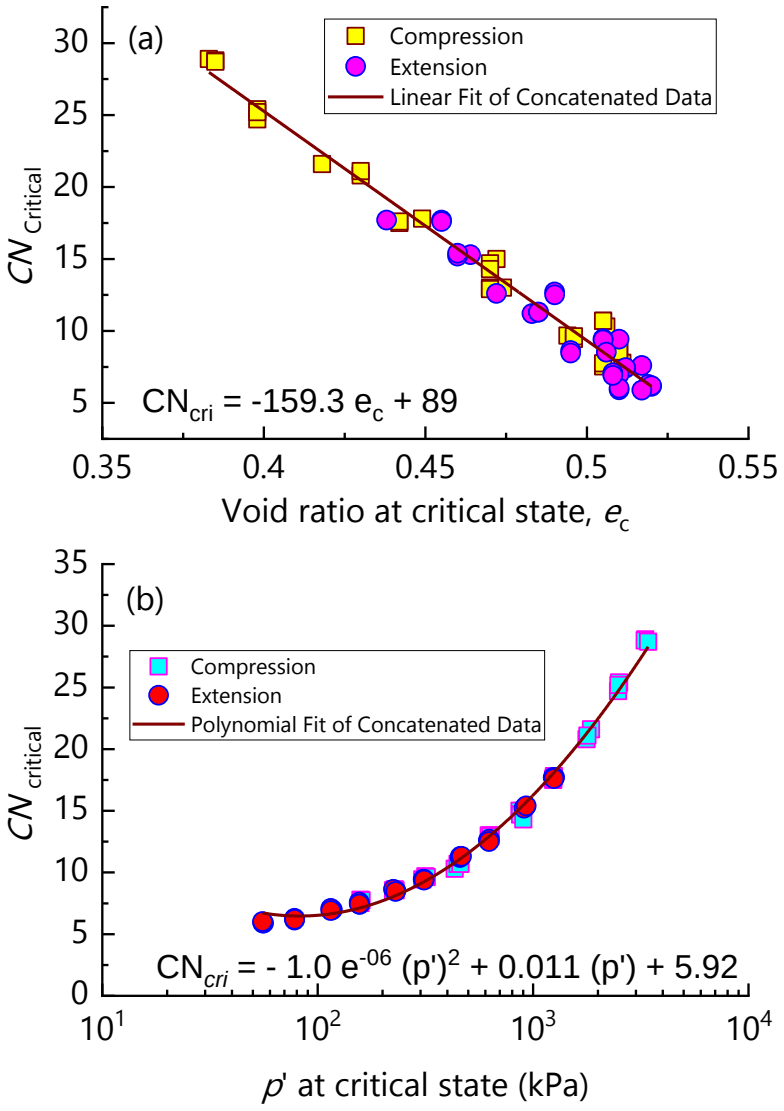

Fig. 11. Relationships of *CN* at critical state: (a) $CN - e_c$; (b) $CN - p'$.

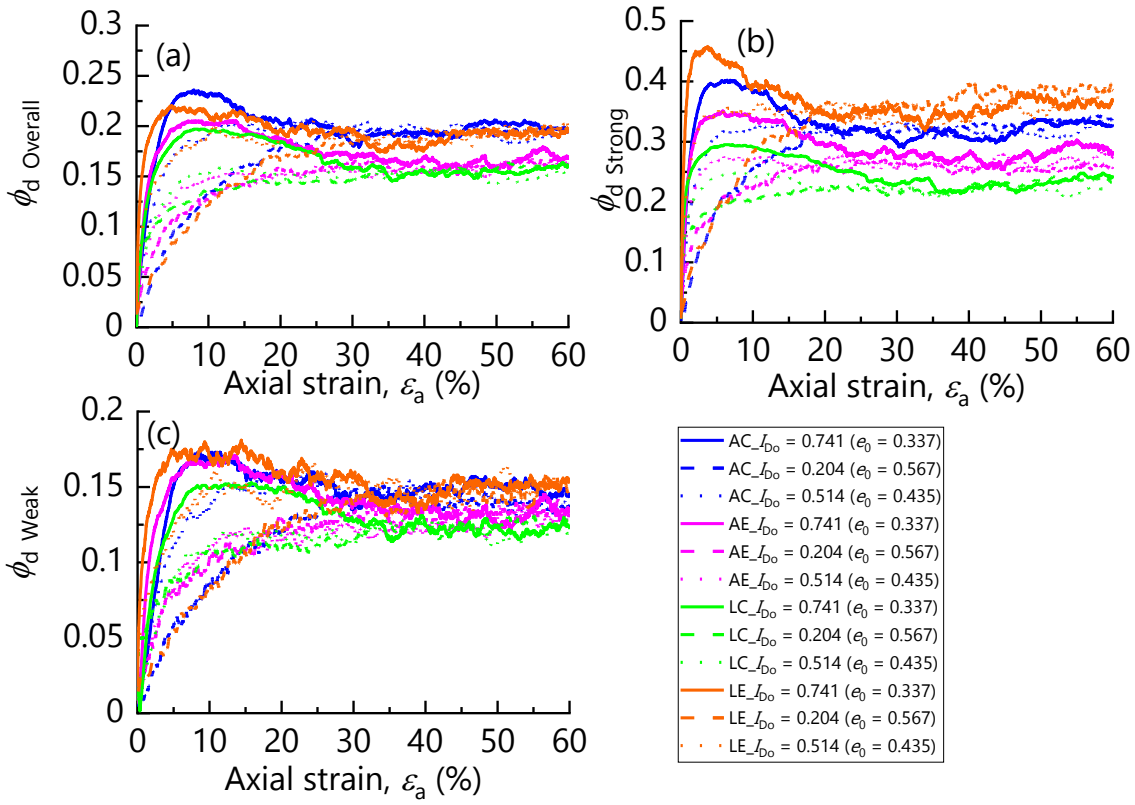

Fig. 12. Evolution of deviator fabrics: (a) $\phi_{d,overall} \sim \varepsilon_a$;(b) $\phi_{d,strong} \sim \varepsilon_a$; (c) $\phi_{d,weak} \sim \varepsilon_a$.

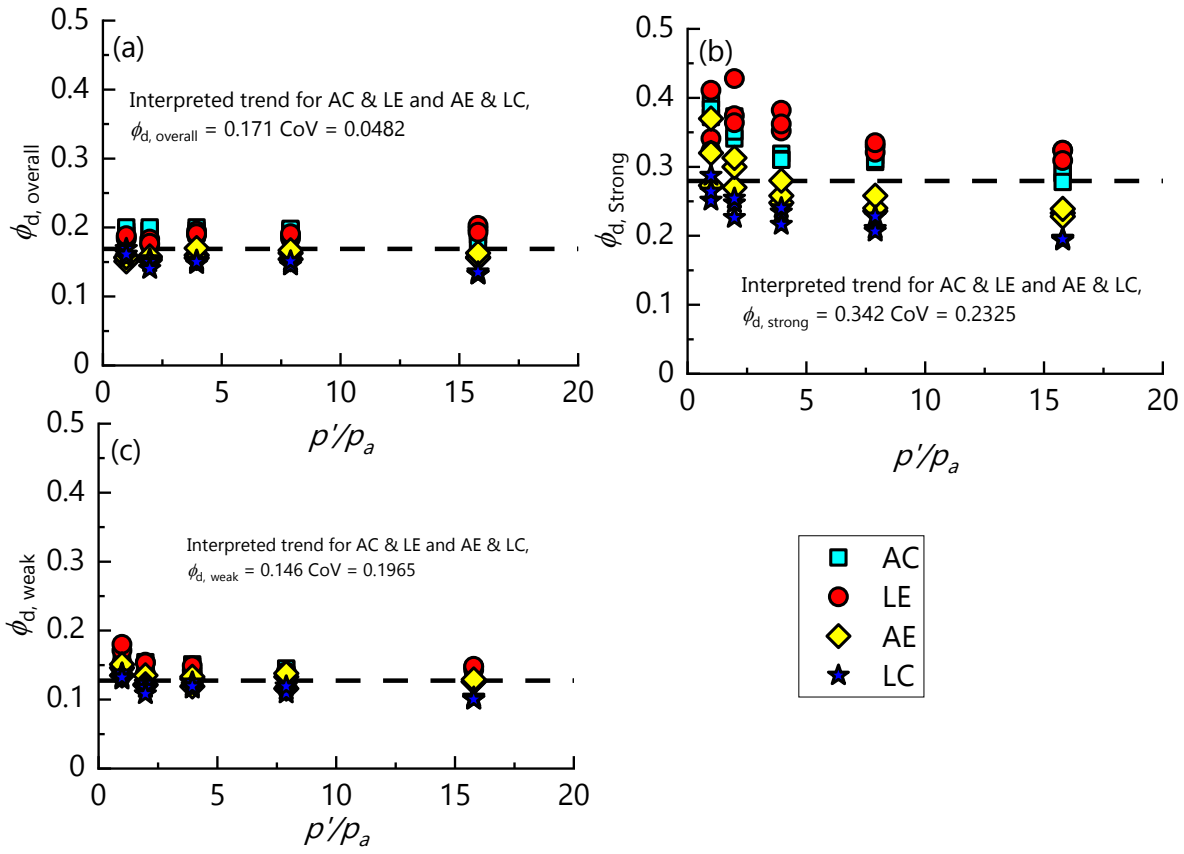

Fig. 13. Evolution of deviator fabrics at critical state: (a) $\phi_{d,overall} \sim \varepsilon_a$;

(b) $\phi_{d,strong} \sim \varepsilon_a$; (c) $\phi_{d,weak} \sim \varepsilon_a$.

Table:

Table 1: Summary of initial characteristics of numerical assemblies

Density classification	Stress path	e_o (p'_o = 100 kPa)	e_o (p'_o = 200 kPa)	e_o (p'_o = 400 kPa)	e_o (p'_o = 800 kPa)	e_o (p'_o = 1600 kPa)
Loose	AC AE LC LE	0.628	0.607	0.567	0.526	0.481
Medium	AC AE LC LE	0.459	0.451	0.434	0.406	0.366
Dense	AC AE LC LE	0.362	0.353	0.336	0.310	0.278